

Electronic Supplementary Information (ESI)

Evolution of Spin-Crossover Transition in Hybrid Crystals Involving Cationic iron Complexes [Fe(III)(3-OMesal₂-trien)]⁺ and Anionic Gold Bis(dithiolene) Complexes Au(dmit)₂ and Au(dddt)₂.

Nataliya G. Spitsyna ¹, Yuri N. Shvachko ^{2*}, Denis V. Starichenko ^{2*}, Erkki Lahderanta ³, Anton A. Komlev ³, Leokadiya V. Zorina ⁴, Sergey V. Simonov ⁴, Maksim A. Blagov ^{1,5}, Eduard B. Yagubskii ¹

1. Synthesis:

[Fe(3-OMe-sal₂-trien)][Au(dmit)₂] (1).

Figure S1 displays the thermogram of [Fe(3-OMe-sal₂-trien)][Au(dmit)₂] (1). A weight loss of 30.08% was observed in the temperature range 120-350°C with DSC endothermic peak at 268.0°C, which is assigned to the melting of 1 and exothermic peak at 277.7°C, which is assigned to the decomposition of the complex (Figure SC). As this takes place, the ions with m/z 18 (H₂O), 17 (HO), 13 (CH) and 26 (CN) relating to the fragments of molecule are observed in the mass spectrum. Figure SD displays the P-XDR 1 in 2θ from 5° to 45°.

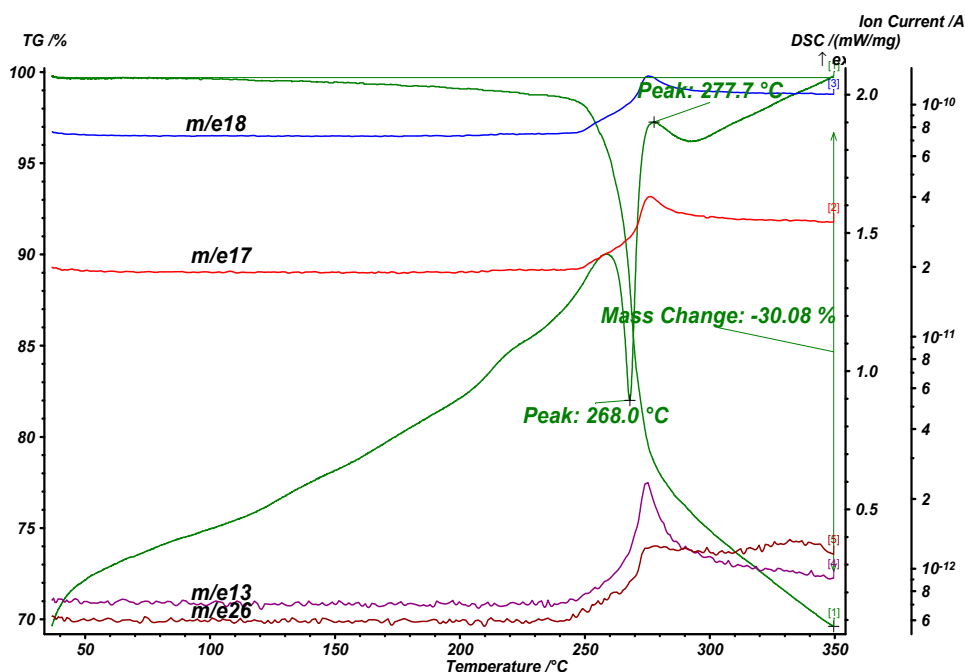


Fig. S1. Thermogravimetric analysis of [Fe(3- OMe-sal₂-trien)][Au(dmit)₂] (1).

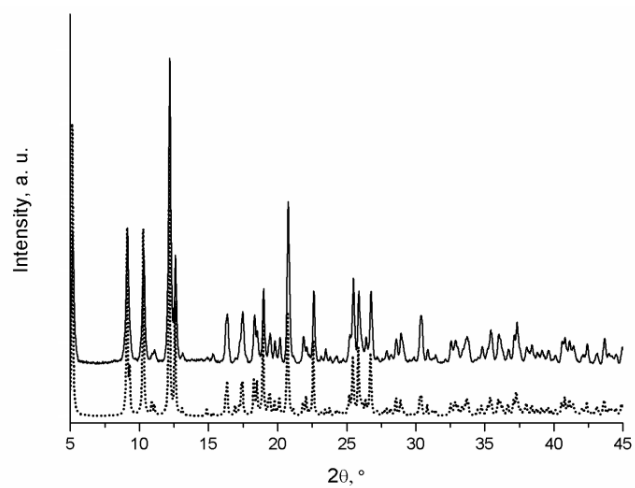


Fig. S2. Powder X-ray diffractogram for [Fe(3-OMe-sal₂-trien)][Au(dmit)₂]: experimental (line) and simulation (dots).

[Fe(3-OMe-sal₂-trien)][Au(ddd_t)₂]-CH₃CN (2).

Figure S3 displays the thermogram of [Fe(3-OMe-sal₂-trien)][Au(ddd_t)₂]-CH₃CN (2).

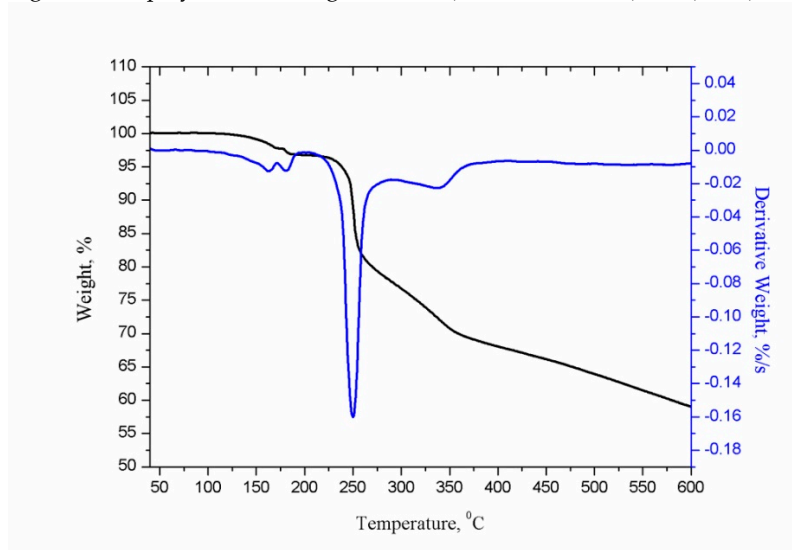


Fig. S3. The thermogravimetric analysis of [Fe(3-OMe-sal₂-trien)][Au(ddd_t)₂]-CH₃CN (2).

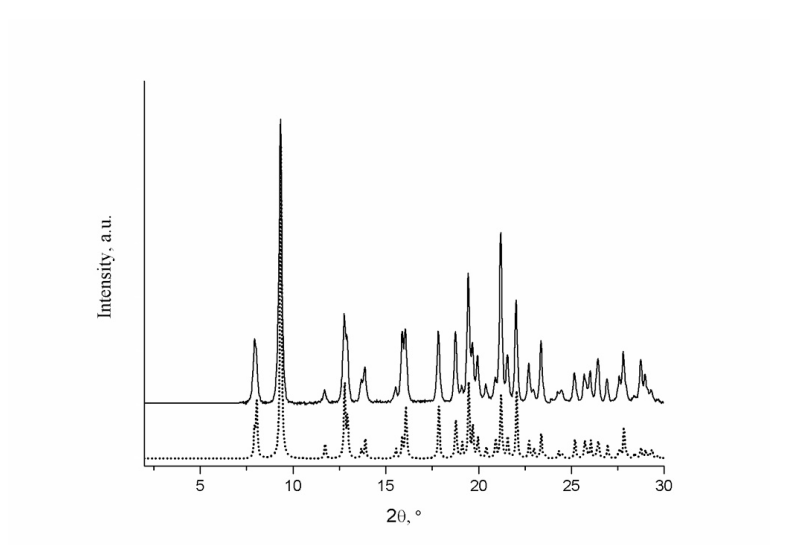


Fig.S4. Powder X-ray diffractogram for [Fe(3-OMe-sal₂-trien)][Au(ddd_t)₂]-CH₃CN: experimental (line) and simulation (dots).

Crystal shapes



Fig. S5. Single crystals of $[\text{Fe}(\text{3-OMesal}_2\text{-trien})][\text{Au}(\text{dmit})_2]$ (left) and $[\text{Fe}(\text{3-OMesal}_2\text{-trien})][\text{Au}(\text{dddt})_2]$ (right).

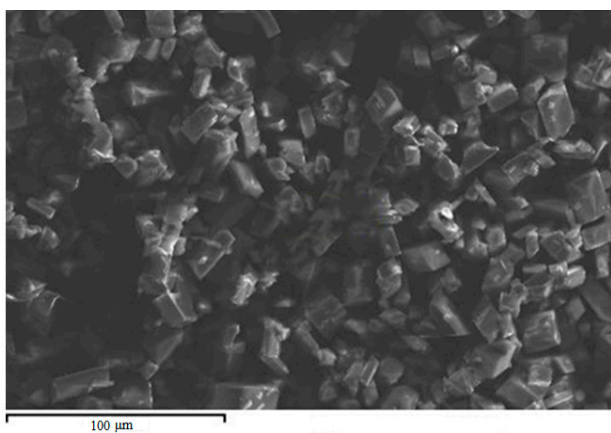


Fig. S6. Polycrystalline sample of $[\text{Fe}(\text{3-OMe-Sal}_2\text{-trien})][\text{Au}(\text{dddt})_2] \cdot \text{CH}_3\text{CN}$

2. Electron-probe X-ray microanalysis (EPMA).

EPMA of the salt crystals was performed with a Zeiss Supra-25 analytical field emission electron microscope equipped with a Gemini electron optical column at magnification varying from 600 to 6200 depending on the sample and the electron beam energy of 9.7-20 keV. The depth of beam penetration into the sample was 1-3 μm .

3. Powder X-Ray Diffraction (*P*-XRD) was measured using a Siemens D500 powder diffractometer with linear detector at room temperature ($\text{CuK}\alpha_1$ - radiation, $\lambda = 1.5406 \text{ \AA}$, step = 0.02° , singlecrystal cuvette). Powder patterns are used as a fingerprint for identification of the crystalline phase presented in a material.

4. Crystal structure determination

X-ray single crystal diffraction studies were carried out on an Oxford Diffraction Gemini-R diffractometer with Atlas CCD detector [$\lambda(\text{MoK}\alpha) = 0.71073 \text{ \AA}$, graphite monochromator, ω -scan mode]. The structures were solved by the direct method and refined by the full-matrix least-squares technique against F^2 in the anisotropic approximation for all non-hydrogen atoms using SHELX-2016 program [1]. Hydrogen atoms were refined isotropically in a rigid model. Table 1 contains unit cell parameters and details of data collection and structure refinement. CCDC 1868121-1, 1868120-1, 1868123-2, 1868122-2 contain supplementary crystallographic data for this paper. These data can be obtained free of charge from the Cambridge Crystallographic Data Centre via www.ccdc.cam.ac.uk/data_request/cif.

5. Thermogravimetric analysis

The thermogravimetric analysis was performed in argon atmosphere with a heating rate $5.0 \text{ }^\circ\text{C min}^{-1}$ using a NETZSCH STA 409 C Luxx thermal analyzer, interfaced to a QMS 403 Aelos mass spectrometer, which allows simultaneous thermogravimetry (TG), differential scanning calorimetry (DSC) and mass-spectrometry measurements.

6. Magnetic SQUID measurements

Magnetic measurements were performed by using a Quantum Design MPMS-5-XL and MPMS-1 SQUID magnetometers. Static magnetic susceptibility $\chi(T)$ was measured on polycrystalline samples at the magnetic field $H = 100 \text{ Oe}$, while warming and cooling regimes. The temperature range of measurements was 2–300 K. Field dependences of the magnetization $M(H)$ were obtained at 2.0 K during several scans over the field range -50 kOe to $+50 \text{ kOe}$. The samples had been cooled down to 2.0 K in the magnetic field $H = 40 \text{ kOe}$. The measurements were performed while decreasing the field value over the sign reversal to -50 kOe and further increasing it to $+50 \text{ kOe}$.

Thermocycling procedure in Fig. 11 corresponds to a series of three subsequent at warming $\chi(T)\uparrow$ and cooling $\chi(T)\downarrow$ cycles shown as black, blue and purple color data points (\circ, \circ, \circ) and respective solid lines guided by mean free path approximation. Solid red line is a reference curve for fresh crystals from Fig. 1.

References

1. Sheldrick, G.M. A short history of SHELX. *Acta Cryst.* **2008**, *A64*, 112-122.